

---

---

# Development and Evaluation of $^{18}\text{F}$ -TTCO-Cys<sup>40</sup>-Exendin-4: A PET Probe for Imaging Transplanted Islets

Zhanhong Wu<sup>1</sup>, Shuanglong Liu<sup>2</sup>, Matthew Hassink<sup>3</sup>, Indu Nair<sup>1</sup>, Ryan Park<sup>2</sup>, Lin Li<sup>4</sup>, Ivan Todorov<sup>1</sup>, Joseph M. Fox<sup>3</sup>, Zibo Li<sup>2</sup>, John E. Shively<sup>4</sup>, Peter S. Conti<sup>2</sup>, and Fouad Kandeel<sup>1</sup>

<sup>1</sup>Department of Diabetes, Endocrinology, and Metabolism, Beckman Research Institute of the City of Hope, Duarte, California;

<sup>2</sup>Molecular Imaging Center, Department of Radiology, University of Southern California, Los Angeles, California; <sup>3</sup>Brown Laboratories, Department of Chemistry and Biochemistry, University of Delaware, Newark, Delaware; and <sup>4</sup>Department of Immunology, Beckman Research Institute of the City of Hope, Duarte, California

---

Because islet transplantation has become a promising treatment option for patients with type 1 diabetes, a noninvasive imaging method is greatly needed to monitor these islets over time. Here, we developed an  $^{18}\text{F}$ -labeled exendin-4 in high specific activity for islet imaging by targeting the glucagonlike peptide-1 receptor (GLP-1R). **Methods:** Tetrazine ligation was used to radiolabel exendin-4 with  $^{18}\text{F}$ . The receptor binding of  $^{19/18}\text{F}$ -tetrazine *trans*-cyclooctene (TTCO)-Cys<sup>40</sup>-exendin-4 was evaluated in vitro with INS-1 cell and in vivo on INS-1 tumor (GLP-1R positive) and islet transplantation models. **Results:**  $^{18}\text{F}$ -TTCO-Cys<sup>40</sup>-exendin-4 was obtained in high specific activity and could specifically bind to GLP-1R in vitro and in vivo. Unlike the radiometal-labeled exendin-4,  $^{18}\text{F}$ -TTCO-Cys<sup>40</sup>-exendin-4 has much lower kidney uptake.  $^{18}\text{F}$ -TTCO-Cys<sup>40</sup>-exendin-4 demonstrated its great potential for transplanted islet imaging: the liver uptake value derived from small-animal PET images correlated well with the transplanted  $\beta$ -cell mass determined by immunostaining. Autoradiography showed that the localizations of radioactive signal indeed corresponded to the distribution of islet grafts in the liver of islet-transplanted mice. **Conclusion:**  $^{18}\text{F}$ -TTCO-Cys<sup>40</sup>-exendin-4 demonstrated specific binding to GLP-1R. This PET probe provides a method to noninvasively image intraportally transplanted islets.

**Key Words:**  $^{18}\text{F}$ -labeled exendin-4; GLP-1R; islet imaging

**J Nucl Med 2013; 54:244–251**

DOI: 10.2967/jnumed.112.109694

---

**N**umerous experimental treatments for type 1 diabetes are currently under development based on strategies includ-

ing immunotherapy, stem cell therapy, and islet transplantation (1). Islet transplantation is much less invasive than whole-pancreas transplantation, which is currently the standard of care in humans. Islet transplantation using the Edmonton protocol can temporarily achieve adequate glycemic control with insulin independence in type 1 diabetes, but to date, only about 10% of the patients maintain insulin independence at 5 y (2). Because of the current lack of tools capable of monitoring islet loss after transplantation, estimates of islet survival and function are limited to indirect assessments based on patients' exogenous insulin requirements or metabolic studies. However, these assessments can be inaccurate because of fluctuations in the metabolic state and insulin secretory capacity of  $\beta$ -cells under different physiologic and pathophysiologic conditions (3,4). A noninvasive method to monitor transplanted islets would provide us the ability to localize the site of transplanted islet engraftment in the liver and to estimate how many islets remain alive and functional over time. This information would be vital to establishing and evaluating the efficiency of pancreatic islet transplantation and graft survival, would likely reveal why some islet cell transplants are successful while others fail, and would facilitate the development of therapies to prolong islet graft survival for all type 1 diabetes patients on a widespread and long-term basis.

There are several challenges in developing an ideal noninvasive and in vivo imaging approach for transplanted islets, primarily due to the small size (50–300  $\mu\text{m}$ ) of pancreatic islets and the relatively low number of transplanted islets engrafted in the whole liver. The ideal imaging modality for islet imaging should be noninvasive, nontoxic to islets, adaptable for serial imaging in the same patient over time, and applicable for clinical translation. PET holds great potential for in vivo islet imaging. PET is a noninvasive functional imaging technique that provides adequate resolution, high sensitivity (capable of detecting tracer molecules in picomolar concentrations), and accurate quantification (relatively simple and reliable) of physiologic, biochemical, and pharmacologic processes in living subjects.

---

Received Jun. 4, 2012; revision accepted Sep. 19, 2012.  
For correspondence or reprints contact either of the following:  
Fouad Kandeel, Department of Diabetes, Endocrinology, and Metabolism, City of Hope, 1500 E. Duarte Rd., Duarte, CA 91010.  
E-mail: fkandeel@coh.org  
Zibo Li, USC Molecular Imaging Center, 2250 Alcazar St., CSC 103, Los Angeles, CA 90033.  
E-mail: ziboli@usc.edu  
Published online Jan. 7, 2013  
COPYRIGHT © 2013 by the Society of Nuclear Medicine and Molecular Imaging, Inc.

Glucagonlike peptide 1 (GLP-1) is an incretin peptide released from the intestine in response to nutrient ingestion; its binding to the GLP-1 receptor (GLP-1R) augments glucose-induced insulin secretion from pancreatic  $\beta$ -cells (5,6). Because GLP-1R localizes to pancreatic duct cells and is expressed in  $\beta$ -cells (7,8), with little to no expression found on other human pancreatic islet cell types (9), properly labeled GLP-1R ligands could serve as ideal probes for pancreatic  $\beta$ -cell imaging. Exendin-4, a peptide hormone first isolated by Dr. John Eng from the saliva of the Gila monster in 1992, is especially attractive as a high-affinity ligand (10–12). Exendin-4 displays biologic properties similar to human GLP-1, with which it shares 53% sequence identity (13); however, it is much more stable metabolically than GLP-1. Previously, exendin analogs have been radiolabeled and evaluated for islet imaging in rodents (14,15) and humans (16). Although these tracers showed great potential for islet imaging, there are 2 major challenges for these probes: first, the high and persistent kidney accumulation of the radiometal-labeled probes may limit their clinical translation because of radiation exposure; second, a probe with high specific activity is needed to avoid blocking effects, as the receptor number is limited. Because of its ideal physical and imaging properties (half-life, 109.8 min;  $\beta^+$ , 97%),  $^{18}\text{F}$  is one of the most extensively used positron emission radionuclides for PET scanning. Although the traditionally used  $^{18}\text{F}$ -labeling method, such as *N*-2-(4- $^{18}\text{F}$ -fluorobenzamido)ethylmaleimide ( $^{18}\text{F}$ -FBEM) (17,18) and  $^{18}\text{F}$ -fluorobenzaldehyde (19), had been used for producing exendin-based tracers, it is difficult to completely separate the  $^{18}\text{F}$ -labeled compound from the precursor as the difference is relatively small and thus may induce a blocking effect to some extent. Recently, an ultra-efficient  $^{18}\text{F}$ -labeling method was developed by our group based on the tetrazine *trans*-cyclooctene (TCO) ligation (20,21). Here, we report the synthesis of  $^{18}\text{F}$ -labeled exendin-4 through this efficient method for *in vivo* imaging of GLP-1 receptor. In addition to characterizing the performance of  $^{18}\text{F}$ -labeled exendin-4 in a rodent insulinoma model, we evaluated its ability to image islet numbers in an intraportal transplanted model.

## MATERIALS AND METHODS

### General

All commercially available chemical reagents were purchased from Aldrich and used without further purification. No-carrier-added  $^{18}\text{F}$ -fluoride was produced via the  $^{18}\text{O}(\text{p,n})^{18}\text{F}$  reaction by the bombardment of an isotopically enriched  $^{18}\text{O}$ -water target (95% enrichment; Isonics) with 11-MeV protons using an RDS-112 negative ion cyclotron (Siemens). Cys $^{40}$ -exendin-4 was purchased from C S Bio, Co.  $^{125}\text{I}$ -exendin(9-39) was purchased from Perkin Elmer. Purification of exendin-4 analogs and  $^{18}\text{F}$ -labeled exendin-4 was performed using a Gemini C18 column (Phenomenex). The flow was set at 1 mL/min, and the mobile phase was changed from 95% solvent A (0.1% trifluoroacetic acid in water) and 5% solvent B (0.1% trifluoroacetic acid in acetonitrile) (0–2 min) to 35% solvent A and 65% solvent B at 32 min.

### Cells

The rat insulinoma cell line INS-1 (GLP-1R–positive, kindly donated by Dr. Ian Sweet, University of Washington) was maintained under standard conditions. The INS-1 insulinoma cells were grown in culture until sufficient cells were available.

Human pancreatic islets were isolated by the Southern California Islet Cell Resources Center from human pancreata of healthy adult donors with proper consent for research use and approval by the Institutional Review Board of the City of Hope. Islets were isolated using the standard collagenase method for pancreas digestion and islet purification (22) following the operating procedures of the Southern California Islet Cell Resources Center. Islets cultured for 48–72 h in CMRL1066-based islet culture medium (Mediatech) were used in the experiments.

### Animals

Male NOD/SCID mice (the City of Hope Animal Resource Center) 8–10 wk old served as recipients for insulinoma cells and human islet cells. All animal experiments were performed in compliance with the Guidelines for the Care and Use of Research Animals established by the City of Hope/Beckman Research Institute's Animal Use Committee.

**Xenograft Tumor Model.** NOD/SCID mice were injected with INS-1 rat insulinoma cells ( $5 \times 10^6$ , suspended in 0.1 mL of 1 $\times$  phosphate-buffered saline) subcutaneously in the thigh. Tumors were established within 18–21 d after injection. Blood glucose values were monitored daily, and 6% glucose solution was fed *ad libitum* once the blood glucose level was lower than 3.3 mM.

**Islet Transplantation.** Islets with a diameter of less than 250  $\mu\text{m}$  were used for transplantation. Islets were transplanted into the livers of NOD/SCID mice via the portal vein. Immediately before intraportal infusion, sham control 500- or 1,000-islet equivalents were suspended in 200  $\mu\text{L}$  of Hanks balanced salt solution (Mediatech) and loaded in a 1-mL syringe. Under general anesthesia, the portal vein was exposed by extraabdominal repositioning of the bowel and the islets were infused into the portal vein via a 27-gauge needle.

### Preparation of Tetrazine-Conjugated Exendin-4 (Tetrazine-Cys $^{40}$ -Exendin-4)

Tetrazine-Mal was prepared as previously reported (21,23). Cys $^{40}$ -exendin-4 (6 mg, 1.4  $\mu\text{mol}$ ) in 100  $\mu\text{L}$  of water was added to tetrazine-Mal (0.7 mg, 1.6  $\mu\text{mol}$ ) in 50  $\mu\text{L}$  of dimethyl sulfoxide (Fig. 1A). The solution was incubated for 30 min at 25°C, and the product was purified by high-performance liquid chromatography (HPLC). The product was characterized by an LTQ FT mass spectrometer (Thermo Scientific) (*m/z* 4,775.19 for  $[\text{MH}]^+$ ,  $\text{C}_{210}\text{H}_{307}\text{N}_{59}\text{O}_{66}\text{S}_2$ , calculated  $[\text{MH}]^+$  4,775.25).

### Preparation of $^{19}\text{F}$ -*Trans*-Cyclooctene-Tetrazine-Conjugated Exendin-4 ( $^{19}\text{F}$ -TCO-Cys $^{40}$ -Exendin-4)

$^{19}\text{F}$ -*trans*-cyclooctene ( $^{19}\text{F}$ -TCO) was prepared according to our previously reported procedure (20).  $^{19}\text{F}$ -TCO (0.5 mg, 3  $\mu\text{mol}$ ) and tetrazine-Cys $^{40}$ -exendin-4 (2 mg, 0.42  $\mu\text{mol}$ ) were incubated at room temperature, and the product was purified by HPLC. The final product was characterized by Thermo LTQ FT mass spectrometry (*m/z* 4,918.38 for  $[\text{MH}]^+$ ,  $\text{C}_{220}\text{H}_{324}\text{FN}_{57}\text{O}_{67}\text{S}_2$ , calculated  $[\text{MH}]^+$  4,918.31).

### Radiochemistry

$^{18}\text{F}$ -TCO was synthesized according to a previously reported procedure (20). Tetrazine-Cys $^{40}$ -exendin-4 (4  $\mu\text{g}$ , 0.84 nmol) was

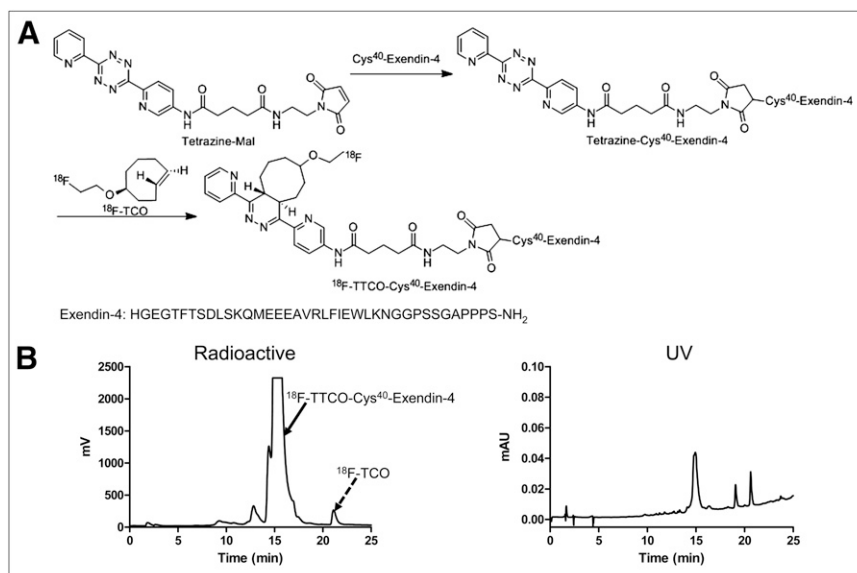


**FIGURE 1.** (A) Synthesis scheme of  $^{18}\text{F}$ -TTCO-Cys<sup>40</sup>-exendin-4. (B) HPLC profiles of crude reaction.

labeled by adding 74 MBq of  $^{18}\text{F}$ -TTCO in 100  $\mu\text{L}$  of acetonitrile followed by 5 min of incubation at room temperature. After dilution with 700  $\mu\text{L}$  of water, the mixture was purified by HPLC. The desired fractions containing  $^{18}\text{F}$ -TTCO-Cys<sup>40</sup>-exendin-4 (Fig. 1B) were combined and rotary evaporated to remove the solvent.  $^{18}\text{F}$ -TTCO-Cys<sup>40</sup>-exendin-4 was then formulated in normal saline for in vivo experiments.

#### Octanol-Water Partition Coefficient

To determine the lipophilicity of  $^{18}\text{F}$ -TTCO-Cys<sup>40</sup>-exendin-4, the final product was diluted in 500  $\mu\text{L}$  of PBS (1 $\times$ ) and an equal volume of octanol was added. After vigorous mixing for 10 min, the mixture was separated by centrifugation (5 min; 5,000 rpm). Counts in aliquots ( $n = 3$ ) of the organic and inorganic layers were determined using a  $\gamma$ -counter (Packard). The log  $P$  values were reported as an average of 2 independent measurements plus the SD.

#### In Vitro Cell-Binding Assay

The in vitro GLP-1R-binding affinity and specificity of  $^{18}\text{F}$ -TTCO-Cys<sup>40</sup>-exendin-4 and exendin-4 were assessed via competitive cell binding assays using  $^{125}\text{I}$ -exendin(9-39) (PerkinElmer) as described previously (14). In detail, INS-1 cells were harvested, washed 3 times with phosphate-buffered saline (1 $\times$ ; Mediatech), and resuspended ( $2 \times 10^6$  cells/mL) in the binding buffer (24). Filter multiscreen DV plates (96-well; pore size, 0.65  $\mu\text{m}$ ; Millipore) were seeded with  $10^5$  cells and incubated with  $^{125}\text{I}$ -exendin(9-39) (0.74 kBq/well) in the presence of increasing concentrations of different exendin-4 analogs (0–1.0  $\mu\text{mol/L}$ ). The truncated exendin(9-39) is an antagonist of GLP-1R and a competitive inhibitor of exendin-4. The total incubation volume was adjusted to 200  $\mu\text{L}$ . After the cells were incubated for 2 h at room temperature, the plates were filtered through a multiscreen vacuum manifold and washed 3 times with binding buffer. The hydrophilic polyvinylidene difluoride filters were collected, and the radioactivity was determined using a  $\gamma$ -counter. The best-fit 50% inhibitory concentration values for INS-1 cells were calculated by fitting the data with nonlinear regression using Prism (GraphPad Software). Experiments were performed on triplicate samples.

#### Histology Study

Human pancreas samples and mouse livers transplanted with human islets were fixed with 10% formalin and processed for paraffin embedding. Parallel sections (5  $\mu\text{m}$ ) were immunostained for insulin, GLP-1R, and glucagon as described previously (9,25). Guinea pig antihuman insulin (DAKO), mouse antihuman glucagon (Sigma), and rabbit antihuman GLP-1R (Novus Biologicals) were used as primary antibodies. The corresponding secondary antibodies were conjugated with fluorescein isothiocyanate or Texas Red (Jackson ImmunoResearch). The slides were counterstained for DNA with diamidinophenylindole (Sigma) and visualized with a BX51 fluorescent microscope (Olympus) equipped with a Pixera CL600 camera.

#### Autoradiography

Ex vivo autoradiography was performed using a Cyclone Storage Phosphor Screen system (Packard) and a Bright 5030/WD/MR cryomicrotome (Hacker Instruments). For the NOD/SCID mouse with intraportally transplanted human islets,  $^{18}\text{F}$ -TTCO-Cys<sup>40</sup>-exendin-4 (3.7 MBq, 0.14  $\mu\text{g}$  peptide) was administered via tail vein injection. The mouse was sacrificed at 1 h after injection, and liver was harvested and frozen immediately. The liver was cut into 10- $\mu\text{m}$  sections, and desired sections were digitally photographed and captured for autoradiography. The sections were transferred into a chilled film cassette containing a Super Resolution screen (spatial resolution, 0.1 mm; Packard) and kept overnight at  $-20^\circ\text{C}$ . The screens were laser-scanned with the Cyclone. After 48 h of radioactive decay, the same sections were fixed with 10% formalin and immunostained for insulin as previously described.

#### Small-Animal PET

Small-animal PET of  $^{18}\text{F}$ -TTCO-Cys<sup>40</sup>-exendin-4 was performed on mice bearing INS-1 tumor or islet grafts to evaluate the in vivo specific binding to GLP-1R. For blocking studies, exendin-4 (20  $\mu\text{g}$ ) was coinjected with the radiotracer. For small-animal PET, the mice were injected via the tail vein with 3.7 MBq ( $\sim 0.14$   $\mu\text{g}$  of peptide) of  $^{18}\text{F}$ -TTCO-Cys<sup>40</sup>-exendin-4. Serial imaging of INS-1 tumor models (at 0.5, 1, 3, and 5 h; scan duration, 5, 5, 5, and 10 min, respectively), islet transplantation models, and control groups

(at 0.5, 1, 2, and 4 h; scan duration, 5, 5, 5, and 10 min, respectively) was performed using a microPET R4 scanner (Concorde Microsystems; 8 cm axial field of view; spatial resolution, 2.0 mm).

Images were reconstructed with a maximum a posteriori iterative algorithm using the microPET Manager Software (Concorde Microsystems). Images were then analyzed using the Acquisition Sino-gram Image Processing software (Concorde Microsystems). Average radioactivity accumulation within the liver was obtained from a 3-dimensional region of interest drawn within the central portion of the PET liver image. Image intensities were converted to units of activity concentration ( $\text{Bq}/\text{cm}^3$ ) using a calibration factor obtained by scanning a cylindrical phantom filled with a known activity concentration of  $^{18}\text{F}$ . Assuming a tissue density of  $1 \text{ g}/\text{mL}$ , measured tissue activity concentrations were converted to units of  $\text{Bq}/\text{g}$  and then multiplied by 100 and divided by the injected dose to obtain an image-derived percentage injected dose per gram of tissue ( $\% \text{ID}/\text{g}$ ).

### Islet Quantification

$\beta$ -cell mass was determined by morphometry on the insulin-immunostained liver sections, as described earlier (26,27). After small-animal PET scanning, the mice were sacrificed and the livers were harvested, weighed, formalin-fixed, and embedded in paraffin. At least 5 parallel sections of  $5\text{-}\mu\text{m}$  thickness were cut  $75 \mu\text{m}$  apart. All sections were immunostained for insulin and hematoxylin and visualized with an IX50 microscope equipped with an DP70 digital microscope camera (Olympus America). The images were analyzed using Microsuite SIS image analysis software (Olympus) in the Measure-Area mode, and the results were converted to volume. The ratio of the volumes for the total insulin-stained areas versus total hematoxylin-stained areas of all sections had been used to calculate the relative volume of  $\beta$ -cells.  $\beta$ -cell mass was determined by multiplying the  $\beta$ -cell relative volume by the total weight of the liver.

### Statistical Analysis

Quantitative data were expressed as mean  $\pm$  SD. Means were compared using 1-way ANOVA and the Student *t* test. *P* values of less than 0.05 were considered statistically significant.

## RESULTS

### Chemistry and Radiolabeling

Conjugation between tetrazine-Mal and Cys<sup>40</sup>-exendin-4 was efficient (75% yield) at room temperature. The identity of tetrazine-Cys<sup>40</sup>-exendin-4 and  $^{19}\text{F}$ -TTCO-Cys<sup>40</sup>-exendin-4 (Fig. 1) was confirmed by HPLC (single peak) and mass spectrometry. The  $^{18}\text{F}$  labeling ( $n = 4$ ) was efficient, and  $^{18}\text{F}$ -TTCO-Cys<sup>40</sup>-exendin-4 was obtained in more than 80% decay-corrected yield with more than 99% radiochemical purity. The total radiosynthesis time was about 90 min from the end of bombardment. The HPLC retention time of  $^{18}\text{F}$ -TTCO-Cys<sup>40</sup>-exendin-4 was 23 min. The specific activity of  $^{18}\text{F}$ -TTCO-Cys<sup>40</sup>-exendin-4 was around  $1.3 \times 10^{17} \text{ Bq}/\text{mol}$ . The log*P* value for  $^{18}\text{F}$ -TTCO-Cys<sup>40</sup>-exendin-4 was determined to be  $-0.14 \pm 0.03$ .

### In Vitro Cell Binding Affinity

We compared the receptor-binding affinity of  $^{19}\text{F}$ -TTCO-Cys<sup>40</sup>-exendin-4 with that of exendin-4 using a competitive cell-binding assay (Fig. 2). Both peptides inhibited the

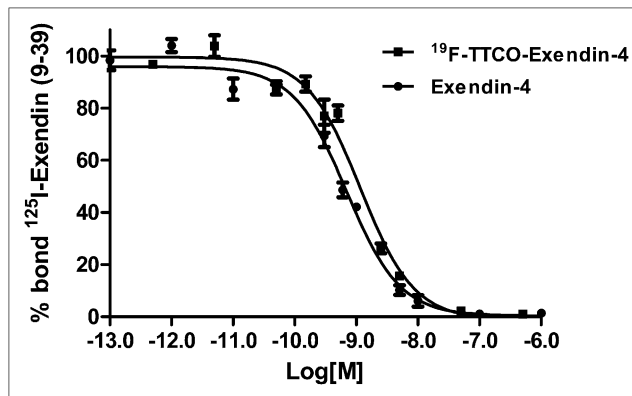


**FIGURE 2.** Competitive binding assays of  $^{125}\text{I}$ -exendin(9-39) and  $^{19}\text{F}$ -TTCO-Cys<sup>40</sup>-exendin-4 or exendin-4 in INS-1 cells. Data are mean  $\pm$  SE ( $n = 3$ ). *x*-axis reflects concentration of nonradiolabeled competitor. For  $^{19}\text{F}$ -TTCO-Cys<sup>40</sup>-exendin-4 and exendin-4, 50% inhibitory concentrations were  $1.17 \pm 0.34$  and  $0.76 \pm 0.19 \text{ nmol}/\text{L}$ , respectively.

binding of  $^{125}\text{I}$ -exendin(9-39) to GLP-1R-positive INS-1 cells in a dose-dependent manner. The 50% inhibitory concentration for  $^{19}\text{F}$ -TTCO-Cys<sup>40</sup>-exendin-4 ( $1.17 \pm 0.34 \text{ nmol}/\text{L}$ ) was comparable to that of exendin-4 ( $0.76 \pm 0.19 \text{ nmol}/\text{L}$ ). The results showed that F-TTCO conjugation had a minimal effect on receptor-binding affinity.

### Histology

The comparison of GLP-1R expression between native human islets and the human islet grafts in mouse liver has been studied. Figure 3 clearly demonstrated that human islet grafts were present in mouse liver and that most GLP-1R-positive cells are also insulin-positive, not glucagon-positive. This observation is consistent with what has been observed for human islets in native pancreas (Fig. 3).

### Small-Animal PET

The GLP-1R targeting efficacy of  $^{18}\text{F}$ -TTCO-Cys<sup>40</sup>-exendin-4 was evaluated in INS-1 insulinoma xenografts (GLP-1R positive) at multiple time points (0.5, 1, 3, and 5 h) with small-animal PET. As shown in Figure 4A, the INS-1 tumors were clearly visualized with high tumor-to-background contrast for  $^{18}\text{F}$ -TTCO-Cys<sup>40</sup>-exendin-4. The tumor uptake was  $12.83 \pm 0.29$ ,  $13.33 \pm 1.12$ ,  $16.03 \pm 1.1$ , and  $12.99 \pm 0.54 \text{ \%ID}/\text{g}$  at 0.5, 1, 3, and 5 h after injection, respectively.

The GLP-1 receptor specificity of  $^{18}\text{F}$ -TTCO-Cys<sup>40</sup>-exendin-4 was confirmed by a blocking experiment in which the radiotracer was coinjected with an excess amount of cold exendin-4 ( $20 \mu\text{g}$ ). As can be seen from Figure 4A, in the presence of unlabeled exendin-4, the INS-1 tumor uptake ( $2.93 \pm 0.35$ ,  $2.47 \pm 0.41$ ,  $1.84 \pm 0.77$ , and  $1.56 \pm 0.16 \text{ \%ID}/\text{g}$  at 0.5, 1, 3, and 5 h after injection, respectively) was significantly ( $P < 0.01$ ) lower than that without exendin-4 blocking at all time points. Figures 4B and 4C showed the quantitative tumor uptake and the ratios of tumor to kidney, liver, and muscle, which were derived from small-animal PET images. The kidney uptake was decreased from

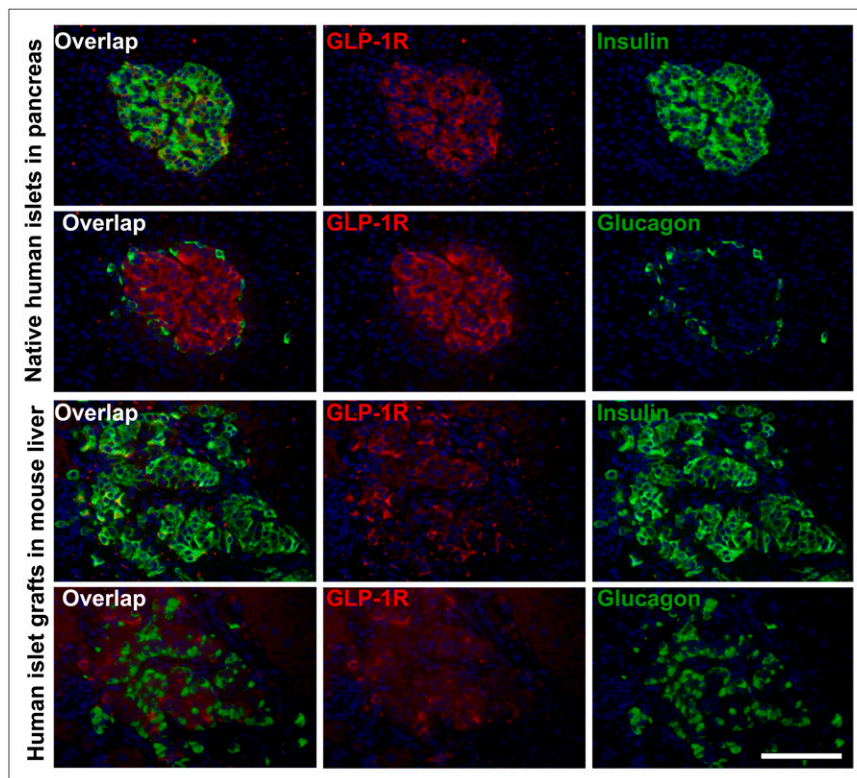


**FIGURE 3.** Human pancreas sections and parallel mouse liver sections were immunostained for GLP-1R, glucagon, and insulin (scale bar, 100  $\mu\text{m}$ ).

$38.24 \pm 6.77$  %ID/g at 0.5 h after injection to  $8.41 \pm 1.40$  %ID/g at 5 h after injection, and the tumor-to-kidney ratio was  $1.58 \pm 0.35$  at 5 h after injection.

On the basis of these promising results, we also tested the tracer in an islet transplant model. 1,000 IEQ human islets were transplanted into mouse liver via the portal vein. For the control mice, only Hanks balanced salt solution was intraportally injected into mice. Twelve days after implantation, mice were imaged with  $^{18}\text{F}$ -TTCO-Cys<sup>40</sup>-exendin-4 (Fig. 4D). The liver uptake of transplanted mice ( $8.25 \pm 0.93$ ,  $7.19 \pm 0.74$ ,  $6.29 \pm 1.03$ , and  $5.17 \pm 0.81$  %ID/g at 0.5, 1, 2, and 4 h after injection, respectively) was significantly higher ( $P < 0.01$ ) than the uptake of control mice ( $4.37 \pm 0.63$ ,  $3.52 \pm 0.33$ ,  $2.85 \pm 0.28$ , and  $1.80 \pm 0.10$  %ID/g at 0.5, 1, 2, and 4 h after injection, respectively) (Fig. 4E). The liver uptake of transplanted mice could be significantly reduced by coinjection of nonradiolabeled exendin-4, thus demonstrating that the increased liver uptake was caused by GLP-1 receptor targeting (Fig. 4F).

To correlate the  $\beta$ -cell mass with imaging intensity, different numbers of human islets were intraportally transplanted into mouse livers and the small-animal PET was performed at 12 d after transplantation. Mice that had been transplanted with 1,000 IEQ human islets had the highest liver uptake when compared with 500 IEQ and sham control groups (Fig. 5A). The liver uptake of the mice transplanted with 500 IEQ human islets was  $4.49 \pm 0.11$  %ID/g, which was significantly lower than uptake in the 1,000 IEQ group ( $7.19 \pm 0.74$  %ID/g) but only slightly higher than that in the control group ( $3.52 \pm 0.33$  %ID/g) (Fig. 5B). The

$\beta$ -cell mass was also evaluated on the basis of the immunostaining (Fig. 5C). As shown in Figures 5B and 5C, the  $\beta$ -cell mass determined from staining correlated well with the uptake value determined from small-animal PET.

#### Ex Vivo Autoradiography

Ex vivo autoradiography was performed with the intraportal islet transplantation model. If the  $^{18}\text{F}$ -TTCO-Cys<sup>40</sup>-exendin-4 were to specifically bind to GLP-1R in vivo, the pattern of radioactivity distribution would match the pattern of GLP-1R expression. As shown in Figure 5D, the localizations of radioactive signal of liver indeed correspond to the distribution of the insulin-positive cells, which are human islet grafts. Because the liver has extremely low GLP-1 receptor expression (7), this result further supported that the increased liver uptake was due to the specific high binding of GLP-1R in human islet grafts in mouse liver.

#### DISCUSSION

GLP-1 receptor has been found to be a good target for islet imaging (28). Previously,  $^{64}\text{Cu}$  (14,15),  $^{68}\text{Ga}$  (29),  $^{99\text{m}}\text{Tc}$  (30), and  $^{111}\text{In}$  (31) have been developed as PET and SPECT tracers for GLP-1R-targeted imaging. Although promising results have been obtained using these methods, persistent and high kidney uptake may ultimately limit their clinical application because of the high radiation exposure to this delicate organ. Another limitation for radiometal-labeled exendin-4 is the need to obtain the tracer in high specific activity. Because the number of GLP-1 receptors is limited in an islet transplantation model (unlike a tumor model),

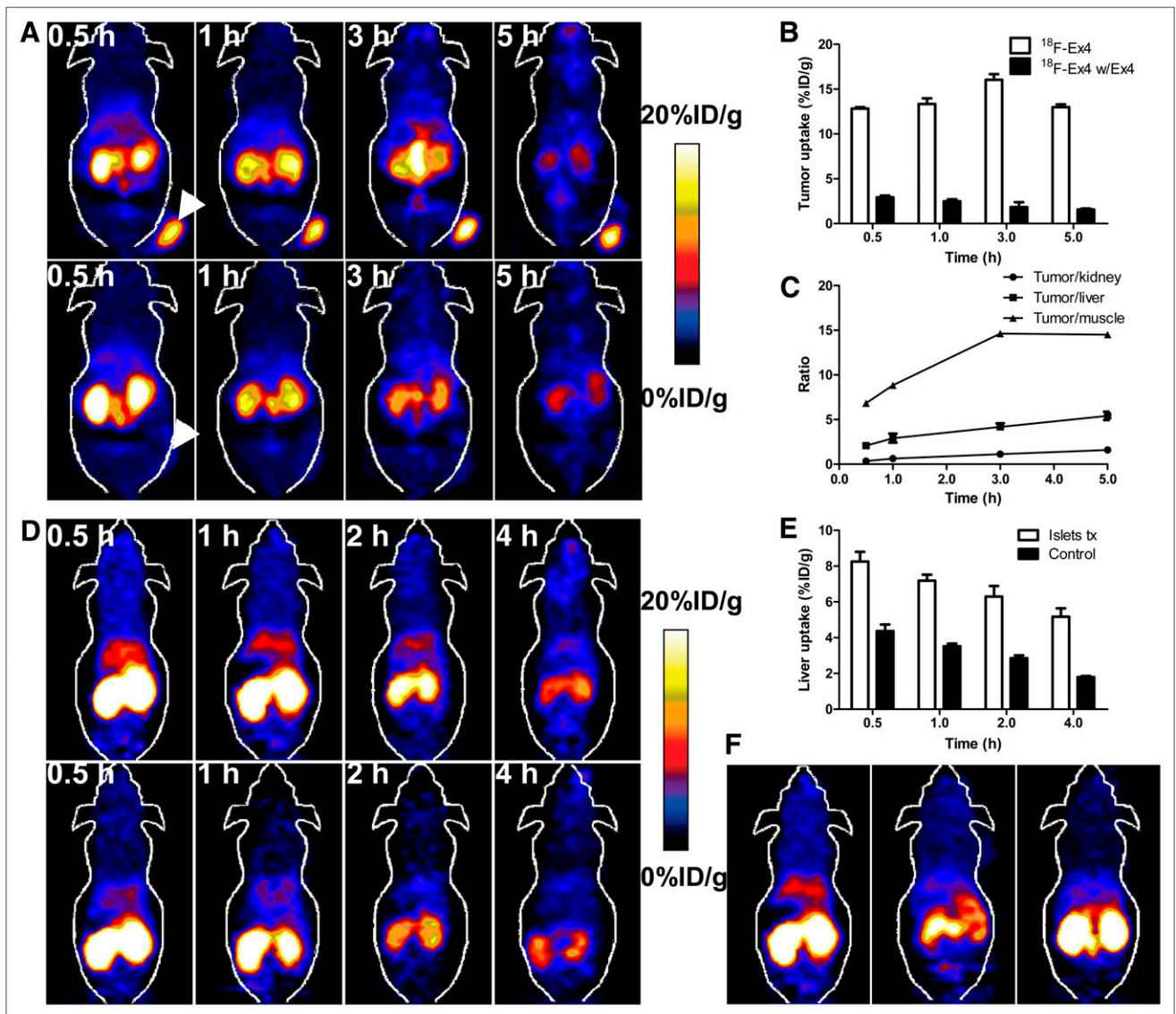


**FIGURE 4.** (A) Representative coronal small-animal PET images of NOD/SCID mice bearing INS-1 xenografts after injection of  $^{18}\text{F}$ -TTCCO-Cys<sup>40</sup>-exendin-4 without (top) and with (bottom) nonradiolabeled exendin-4 (arrows point to tumor). (B) Comparison of tumor uptakes between control and blocking groups. Data were derived from multiple time-point small-animal PET study. ROIs are shown as %ID/g  $\pm$  SD ( $n = 3$ ). (C) Comparison of tumor to muscle, kidney, and liver ratios of  $^{18}\text{F}$ -TTCCO-Cys<sup>40</sup>-exendin-4 at different time points after injection ( $n = 3$ , mean  $\pm$  SD). (D) Representative coronal small-animal PET images of  $^{18}\text{F}$ -TTCCO-Cys<sup>40</sup>-exendin-4 in NOD/SCID mice transplanted with human islets into liver (top) and control mice (bottom) at 0.5, 1, 2, and 4 h after injection. (E) Comparison of liver uptake between intraportal islet transplantation and sham control groups. Data were derived from multiple time-point small-animal PET study. ROIs are shown as %ID/g  $\pm$  SD ( $n = 3$ ). (F) Representative coronal small-animal PET images of mice transplanted with human islets (left:  $^{18}\text{F}$ -TTCCO-Cys<sup>40</sup>-exendin-4; middle: coinjection with nonradiolabeled exendin-4) and sham control mice (right: coinjection with nonradiolabeled exendin-4) at 1 h after injection.

a minimal amount of unlabeled exendin-4 is able to saturate GLP-1R, leading to a blocking effect (29). Therefore, a tracer with high specific activity is necessary to obtain accurate information from islet imaging.

$^{18}\text{F}$  is the most widely used PET isotope. Because of its short half-life and low energy range,  $^{18}\text{F}$  would be a promising option to reduce kidney radiation exposure. Moreover,  $^{18}\text{F}$  could be obtained in extremely high specific activity, which could lead to a final PET tracer of high specific activity. With traditional  $^{18}\text{F}$ -labeling methods, such as  $^{18}\text{F}$ -FBEM

or  $^{18}\text{F}$ -fluorobenzaldehyde, excess amounts of peptide (notably, a relatively large amount of peptide compared with  $^{18}\text{F}$ -FBEM or  $^{18}\text{F}$ -fluorobenzaldehyde) are needed to obtain a reasonable radiolabeling yield. Because of the similarities between  $^{18}\text{F}$ -labeled exendin-4 and unlabeled exendin-4, it is difficult to completely separate them by HPLC, which means the GLP-1 receptor could be partially blocked by unlabeled exendin-4, especially in an islet transplantation model. Although  $^{18}\text{F}$ -labeled exendin-4 has been studied recently by other groups, these probes were tested only

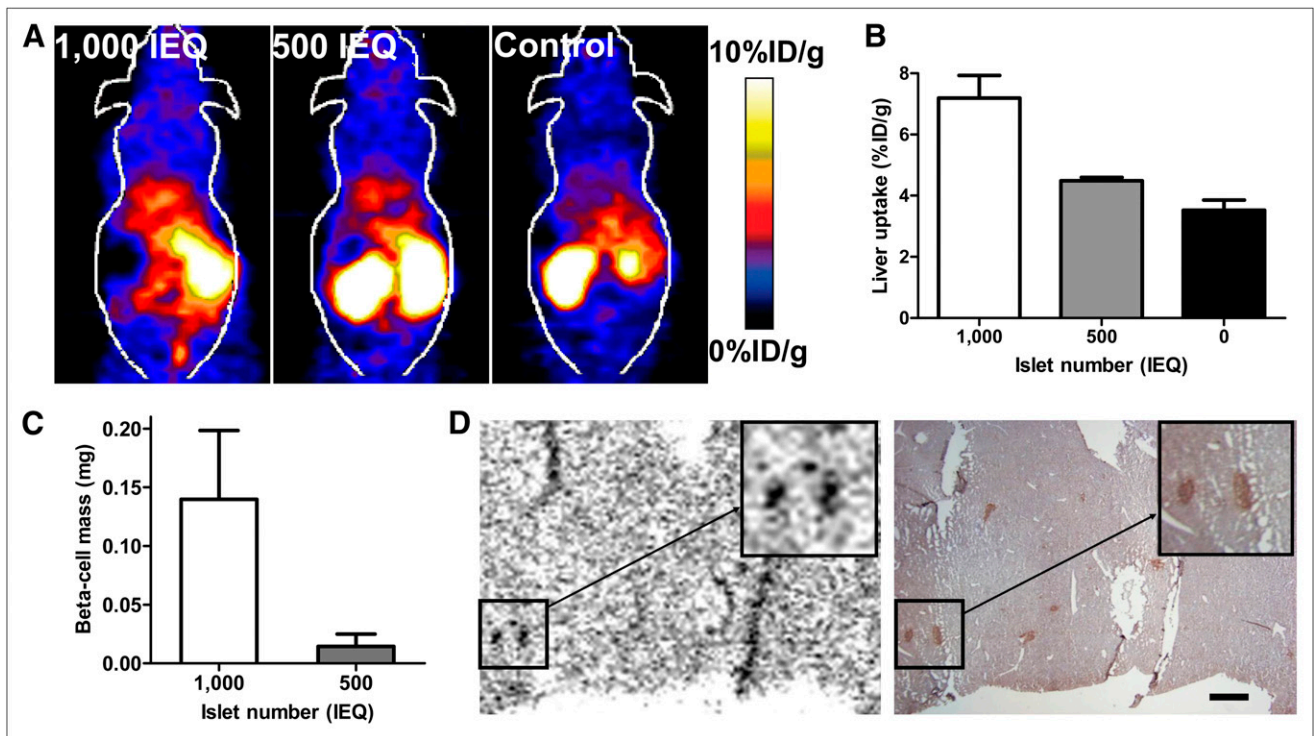


**FIGURE 5.** (A) Representative in vivo small-animal PET images of intraportal islet transplantation and control groups at 1 h after injection. (B) Comparison of liver uptake between intraportal islet transplantation groups (1,000 IEQ,  $n = 5$ ; 500 IEQ,  $n = 4$ ) and control group ( $n = 5$ ). (C)  $\beta$ -cell mass quantification result determined by immunohistologic staining. (D) Ex vivo autoradiography (left) of human islet graft in mouse liver and corresponding insulin immunohistochemical staining (right) of same slide (scale bar, 1,000  $\mu$ m).

in an INS-1 tumor model (18) or in an STZ-induced diabetic rodent model (19), in which suboptimal results were obtained (likely caused by blocking effects due to insufficient elimination of unlabeled exendin-4). Unlike the INS-1 tumor model, the GLP-1R would be limited in the islet transplantation model or native pancreas. Clearly, obtaining the radiotracer in high specific activity is the key factor for the success of islet imaging, and an efficient labeling approach is needed. Recently, based on the ultra-efficient tetrazine-TCO ligation method,  $^{18}\text{F}$ -labeled tracers have been produced at high yield with both reagents at dilute concentrations. This reaction provides us an unprecedented opportunity to produce an  $^{18}\text{F}$ -labeled exendin-4 with high specific activity. In our research, tetrazine was conjugated to the exendin-4 site specifically through a thiol-maleimide reaction. For  $^{18}\text{F}$  labeling, we are surprised to find that tetrazine-Mal-Cys<sup>40</sup>-exendin-4 could react with  $^{18}\text{F}$ -TCO in an almost 1:1 ratio at room temperature with a radiolabeling yield of more than 80%. This extremely high labeling efficiency allows us to produce the final probe with high specific activity. The receptor binding affinity of  $^{19}\text{F}$ -TTTCO-Cys<sup>40</sup>-exendin-4 was evaluated in vitro, and the TTTCO ligation was demonstrated to have a minimal effect on receptor binding. The following small-animal PET images in the INS-1 tumor model demonstrated that  $^{18}\text{F}$ -TTTCO-Cys<sup>40</sup>-exendin-4 could also specifically bind to GLP-1 receptor in vivo. Moreover, unlike the radiometal-labeled exendin-4 analogs,  $^{18}\text{F}$ -TTTCO-Cys<sup>40</sup>-

exendin-4 has a much lower kidney uptake and faster clearance rate. The kidney uptake was  $22.4 \pm 5.3$  %ID/g and  $8.4 \pm 1.4$  %ID/g for  $^{18}\text{F}$ -TTTCO-Cys<sup>40</sup>-exendin-4 at 1 and 5 h after injection, compared with  $79.7 \pm 6.83$  and  $46.8 \pm 11.4$  %ID/g for  $^{64}\text{Cu}$ -DO3A-VS-Cys<sup>40</sup>-exendin-4 at 4 and 23 h after injection (14). The kidney has low GLP-1R expression, and the blocking study demonstrated that the high kidney uptake could not be significantly reduced by cold exendin-4. Although the reason for the slower kidney clearance of radiometal-labeled exendin-4 was not investigated, it is likely due to the difference in metabolism after reabsorption by the tubules (see Li et al. (32) on radiometal retention in the kidneys for radiometal/labeled antibodies). Clearly,  $^{18}\text{F}$ -TTTCO-Cys<sup>40</sup>-exendin-4 not only could be obtained in high specific activity but also significantly reduced the kidney exposure compared with the radiometal-labeled counterparts (14,29–31).

Because our ultimate goal is to image transplanted islets,  $^{18}\text{F}$ -TTTCO-Cys<sup>40</sup>-exendin-4 was then evaluated in the transplantation model to quantify  $\beta$ -cell mass. Because liver is currently the most common site for clinical islet transplantation, human islets were therefore transplanted into NOD/SCID mouse livers in our model. Although 1,000 or 500 IEQ human islets are an extremely small amount of cells compared with those residing within the entirety of the liver (the ratio of transplanted islets to liver cells is around 1:10,000), we still observed the increased liver uptake by targeting

GLP-1R in islet grafts at 12 d after transplantation compared with control (nontransplanted) mice. Blocking experiments clearly demonstrated the specificity of this increase. The  $\beta$ -cell mass was also determined by immunostaining and correlated with the liver uptake derived from small-animal PET images. The  $\beta$ -cell mass of the mice transplanted with 1,000 IEQ islets ( $1.83 \pm 0.84$  mg) was higher than that of the mice transplanted with 500 IEQ islets ( $0.46 \pm 0.05$  mg). These results correlate well with small-animal PET images: the liver uptake of the 1,000 IEQ group was higher than that of the 500 IEQ and control groups. Meanwhile, ex vivo autoradiography also clearly demonstrated that the distribution patterns of  $^{18}\text{F}$ -TTCO-Cys<sup>40</sup>-exendin-4 in liver correlated well with the GLP-1 receptor distribution pattern.

## CONCLUSION

GLP-1R could be a robust target for imaging transplanted islets.  $^{18}\text{F}$ -TTCO-Cys<sup>40</sup>-exendin-4 could be obtained in extremely high specific activity through ultra-efficient TTCO ligation. This probe showed high and specific binding affinity to GLP-1R in vivo and much lower kidney uptake than is seen with radiometal-labeled exendin. Moreover, it has been demonstrated that  $^{18}\text{F}$ -TTCO-Cys<sup>40</sup>-exendin-4 is capable of imaging intraportally transplanted islets. These results suggest that  $^{18}\text{F}$ -TTCO-Cys<sup>40</sup>-exendin-4 is a promising PET probe for noninvasively imaging intraportally transplanted pancreatic islets in clinical practice.

## DISCLOSURE

The costs of publication of this article were defrayed in part by the payment of page charges. Therefore, and solely to indicate this fact, this article is hereby marked "advertisement" in accordance with 18 USC section 1734. This work was supported by the Juvenile Diabetes Research Foundation International (JDRF-37-2009-20) and the Jonas Bros Foundation. No potential conflict of interest relevant to this article was reported.

## ACKNOWLEDGMENT

We thank Dr. Ismail Al-Abdullah and the islet isolation team of the Southern California Islet Cell Resource Center at City of Hope for providing the human islets. We thank Stephen Scott for his technical support.

## REFERENCES

- van Belle TL, Coppieters KT, von Herrath MG. Type 1 diabetes: etiology, immunology, and therapeutic strategies. *Physiol Rev*. 2011;91:79–118.
- Langer RM. Islet transplantation: lessons learned since the Edmonton breakthrough. *Transplant Proc*. 2010;42:1421–1424.
- Shapiro AM, Hao EG, Lakey JR, et al. Novel approaches toward early diagnosis of islet allograft rejection. *Transplantation*. 2001;71:1709–1718.
- Shapiro AM, Lakey JR, Ryan EA, et al. Islet transplantation in seven patients with type 1 diabetes mellitus using a glucocorticoid-free immunosuppressive regimen. *N Engl J Med*. 2000;343:230–238.
- Holst JJ. The physiology of glucagon-like peptide 1. *Physiol Rev*. 2007;87:1409–1439.
- Baggio LL, Drucker DJ. Biology of incretins: GLP-1 and GIP. *Gastroenterology*. 2007;132:2131–2157.

- Körner M, Stockli M, Waser B, Reubi JC. GLP-1 receptor expression in human tumors and human normal tissues: potential for in vivo targeting. *J Nucl Med*. 2007;48:736–743.
- Moens K, Heimberg H, Flamez D, et al. Expression and functional activity of glucagon, glucagon-like peptide I, and glucose-dependent insulinotropic peptide receptors in rat pancreatic islet cells. *Diabetes*. 1996;45:257–261.
- Tornehave D, Kristensen P, Romer J, Knudsen LB, Heller RS. Expression of the GLP-1 receptor in mouse, rat, and human pancreas. *J Histochem Cytochem*. 2008;56:841–851.
- Eng J, Kleinman WA, Singh L, Singh G, Raufman JP. Isolation and characterization of exendin-4, an exendin-3 analogue, from *Heloderma suspectum* venom: further evidence for an exendin receptor on dispersed acini from guinea pig pancreas. *J Biol Chem*. 1992;267:7402–7405.
- Edwards CM, Stanley SA, Davis R, et al. Exendin-4 reduces fasting and postprandial glucose and decreases energy intake in healthy volunteers. *Am J Physiol Endocrinol Metab*. 2001;281:E155–E161.
- Malhotra R, Singh L, Eng J, Raufman JP. Exendin-4, a new peptide from *Heloderma suspectum* venom, potentiates cholecystokinin-induced amylase release from rat pancreatic acini. *Regul Pept*. 1992;41:149–156.
- Göke R, Fehmann HC, Linn T, et al. Exendin-4 is a high potency agonist and truncated exendin-(9-39)-amide an antagonist at the glucagon-like peptide 1-(7-36)-amide receptor of insulin-secreting beta-cells. *J Biol Chem*. 1993;268:19650–19655.
- Wu Z, Todorov I, Li L, et al. In vivo imaging of transplanted islets with <sup>64</sup>Cu-DO3A-VS-Cys<sup>40</sup>-exendin-4 by targeting GLP-1 receptor. *Bioconjug Chem*. 2011;22:1587–1594.
- Connolly BM, Vanko A, McQuade P, et al. Ex vivo imaging of pancreatic beta cells using a radiolabeled GLP-1 receptor agonist. *Mol Imaging Biol*. 2012;14:79–87.
- Pattou F, Kerr-Conte J, Wild D. GLP-1-receptor scanning for imaging of human beta cells transplanted in muscle. *N Engl J Med*. 2010;363:1289–1290.
- Gao H, Niu G, Yang M, et al. PET of insulinoma using <sup>18</sup>F-FBEM-EM3106B, a new GLP-1 analogue. *Mol Pharm*. 2011;8:1775–1782.
- Kiesewetter DO, Gao H, Ma Y, et al. <sup>18</sup>F-radiolabeled analogs of exendin-4 for PET imaging of GLP-1 in insulinoma. *Eur J Nucl Med Mol Imaging*. 2012;39:463–473.
- Wang Y, Lim K, Normandin M, Zhao X, Cline GW, Ding YS. Synthesis and evaluation of [<sup>18</sup>F]exendin (9-39) as a potential biomarker to measure pancreatic beta-cell mass. *Nucl Med Biol*. 2012;39:167–176.
- Li Z, Cai H, Hassink M, et al. Tetrazine-trans-cyclooctene ligation for the rapid construction of <sup>18</sup>F labeled probes. *Chem Commun (Camb)*. 2010;46:8043–8045.
- Liu S, Hassink M, Selvara R, et al. Ultra-efficient <sup>18</sup>F labeling of cysteine containing peptides and proteins. *Mol Imaging*. In press.
- Ricordi C, Lacy PE, Scharp DW. Automated islet isolation from human pancreas. *Diabetes*. 1989;38(suppl 1):140–142.
- Blackman ML, Royzen M, Fox JM. Tetrazine ligation: fast bioconjugation based on inverse-electron-demand Diels-Alder reactivity. *J Am Chem Soc*. 2008;130:13518–13519.
- Gallwitz B, Witt M, Folsch UR, Creutzfeldt W, Schmidt WE. Binding specificity and signal transduction of receptors for glucagon-like peptide-1(7-36)amide and gastric inhibitory polypeptide on RINm5F insulinoma cells. *J Mol Endocrinol*. 1993;10:259–268.
- Todorov I, Nair I, Avakian-Mansoorian A, et al. Quantitative assessment of beta-cell apoptosis and cell composition of isolated, undisturbed human islets by laser scanning cytometry. *Transplantation*. 2010;90:836–842.
- Zhang C, Todorov I, Lin CL, et al. Elimination of insulinitis and augmentation of islet beta cell regeneration via induction of chimerism in overtly diabetic NOD mice. *Proc Natl Acad Sci U S A*. 2007;104:2337–2342.
- Montaña E, Bonner-Weir S, Weir GC. Beta cell mass and growth after syngeneic islet cell transplantation in normal and streptozocin diabetic C57BL/6 mice. *J Clin Invest*. 1993;91:780–787.
- Behnam Azad B, Rota VA, Breadner D, Dhanvantari S, Luyt LG. Design, synthesis and in vitro characterization of glucagon-like peptide-1 derivatives for pancreatic beta cell imaging by SPECT. *Bioorg Med Chem*. 2010;18:1265–1272.
- Brom M, Oyen WJ, Joosten L, Gotthardt M, Boerman OC. <sup>68</sup>Ga-labelled exendin-3, a new agent for the detection of insulinomas with PET. *Eur J Nucl Med Mol Imaging*. 2010;37:1345–1355.
- Wild D, Wicki A, Mansi R, et al. Exendin-4-based radiopharmaceuticals for glucagonlike peptide-1 receptor PET/CT and SPECT/CT. *J Nucl Med*. 2010;51:1059–1067.
- Wild D, Behe M, Wicki A, et al. [<sup>18</sup>F]Lys40(Ahx-DTPA-<sup>111</sup>In)NH<sub>2</sub>exendin-4, a very promising ligand for glucagon-like peptide-1 (GLP-1) receptor targeting. *J Nucl Med*. 2006;47:2025–2033.
- Li L, Olafsen T, Anderson AL, et al. Reduction of kidney uptake in radiometal labeled peptide linkers conjugated to recombinant antibody fragments: site-specific conjugation of DOTA-peptides to a Cys-diabody. *Bioconjug Chem*. 2002;13:985–995.